Auger decay of the photoexcited $2p^{-1}nl$ Rydberg series in argon

T. W. Gorczyca
Department of Physics, Western Michigan University, Kalamazoo, Michigan 49008-5151

F. Robicheaux
Department of Physics, Auburn University, Auburn, Alabama 36849-5311

(Received 28 January 1999)

The $2p^{-1}ns(nd)$ inner-shell photoexcited resonance states in argon are studied using a combination of optical potential, multichannel quantum defect theoretical, and *R*-matrix methods. Optical potential inclusion of the infinite number of core decay channels correctly accounts, in an implicit manner, for the physical broadening of resonances within the $3p^{-1}$ and $3s^{-1}$ cross sections, but highly asymmetric resonance features remain. Comparison with experimental results is made, showing good qualitative agreement in the resonance profiles. The quantitative differences are due to unconverged theoretical resonance energies and to discrepancies in the background cross sections. Fine-structure-resolved cross sections and angular distribution parameters are investigated in the present calculations, revealing major qualitative departure from nonrelativistic predictions; these features should be observable in high-resolution measurements. [S1050-2947(99)09308-7]

PACS number(s): 32.80.Hd, 32.80.Rm

I. INTRODUCTION

Photoionization of the rare gases has provided a convenient testing ground for atomic many-body theory due to the wealth of experimental measurements available [1–3]. Among the various methods at the forefront of theoretical photoionization studies are those based on the close-coupling expansion [4], for instance, the widely used *R*-matrix method [3,5]. In this approach, the scattering wave function is necessarily expanded in terms of a finite basis. Most photoionization studies using close-coupling methods have focused on outer-shell processes, due to restrictions on the size of the basis set.

An excited state with a hole in an inner shell can often decay into an infinite number of open channels via Auger decay, and all of these channels cannot be included within an explicit close-coupling expansion. The purpose of the present study is to treat the resonance region in argon where there is a hole in the $2p$ shell. We combine optical potential considerations and multichannel quantum defect theory (MQDT), within *R*-matrix calculations, to overcome the difficulties associated with the infinite number of open channels.

In a single configuration description, the following states are accessible following photoabsorption by the argon ground state of a photon in the energy range 244 eV$\lesssim h\nu \lesssim$251 eV:

$$h\nu + 2p^6 3s^2 3p^6 \rightarrow 2p^6 3s^2 3p^5 \epsilon s,d \quad (3p^{-1} \text{ main line}) \tag{1}$$

$$\rightarrow 2p^6 3s 3p^6 \epsilon p \quad (3s^{-1} \text{ main line}) \tag{2}$$

$$\rightarrow 2p^5 3s^2 3p^6 ns,nd \quad \text{(inner-shell excited resonances)}. \tag{3}$$

Even within this single-configuration description, excitation of the $2p$ subshell makes up an allowed contribution to the high-energy photoionization cross section. A standard, simplified *R*-matrix approach for theoretically determining the photoionization cross sections to the so called *main lines* in Eqs. (1) and (2) might be the following. The first three open channels in Eqs. (1) and (2) and the latter two closed channels in Eq. (3) are included in the close-coupling expansion, the *R*-matrix and scattering and dipole matrices are computed within this basis, and the photoionization cross sections to the $3s^2 3p^5$ and $3s 3p^6$ continua are determined. Important physics is neglected in such a calculation, however; consider the possible autoionization pathways of an intermediate (nd) resonance state:

$$2p^5 3s^2 3p^6 nd \rightarrow 2p^6 3s^i 3p^j \epsilon l \quad (i+j=7) \quad (\textit{participator} \text{ Auger decay to main lines}), \tag{4}$$

$$\rightarrow 2p^6 3s^i 3p^j nd\, \epsilon l \quad (i+j=6) \quad (\textit{spectator} \text{ Auger decay to satellite lines}). \tag{5}$$

In participator Auger decay, the valence electron orbital nd appears in the autoionization matrix element, so the partial decay width scales with the principal quantum number as $\Gamma_p \sim n^{-3}$; this is accounted for by the explicit inclusion of the $2p^6 3s^2 3p^5$ and $2p^6 3s 3p^6$ target states in the close-coupling expansion. Spectator decay to the *satellite* lines, on the other hand, does not involve the valence electron in the autoionization matrix element, so the partial decay width is

independent of the principal quantum number ($\Gamma_s \sim n^0$). Spectator decay therefore dominates the photoionization process at higher n.

It is necessary to consider the spectator decay channels in the theoretical treatment, but this presents a difficulty for close-coupling methods, due to the infinite number of $2p^6 3s^i 3p^j nd$ states accessible when studying the Rydberg series $n \to \infty$. In fact, inclusion of these states is impractical even for a single n, because there are 22 $L_c S_c$ terms derived from the $3s^i 3p^j 3d$ Ar^+ configurations, leading to 53 J_c levels. An R-matrix calculation of this size would strain the limits of most computers, and would still neglect important physics. Fortunately, the strong dependence of spectator Auger decay on the core transitions, rather than on the properties of the valence electron, suggests the use of optical potential methods to include spectator Auger decay channels in an implicit manner.

Our primary goal is to investigate photoionization to the participator channels near the argon $2p^{-1}$ inner-shell threshold. It is important to consider interference between the direct photoionization pathways in Eqs. (1) and (2), and the resonant photoionization pathways in Eqs. (3) and (4), since both are allowed contributions even within the single configuration approximation, and the R-matrix method handles this explicitly. Dominance of spectator decay in Eq. (5) leads to a broadening and reduction, or *damping*, of the resonance profile in the participator channels, and this effect needs to be accounted for within the theoretical treatment. In Sec. II, various theoretical methods are outlined for accomplishing this, including optical potential, MQDT, and R-matrix techniques. The appendixes supplement this section with certain technical derivations of the relevant equations used. Computational details are given in Sec. III, then in Sec. IV theoretical results are compared to experimental ones for the participator and total cross sections. Theoretical fine-structure-resolved cross sections and angular distribution parameters β are also presented, demonstrating the significance of the spin-orbit interaction on the qualitative resonance behavior. Concluding remarks follow in Sec. V.

II. THEORETICAL METHODS

The starting point of the theoretical formulation is the widely used R-matrix method [5], which expands the total wavefunction in terms of the following basis Ψ_k:

$$\Psi_k = \mathcal{A} \sum_i \Phi_i(R) \sum_j c_{ijk} u_{ij}(r) + \sum_\alpha d_{\alpha k} \chi_\alpha(R,r). \quad (6)$$

Here $\Phi_i(R)$ are configuration-interaction (CI) wave functions for the target ionic states, $u_{ij}(r)$ are basis functions for the outer electron's orbital, $\mathcal{A}$ is an antisymmetrization operator, and the coefficients c_{ijk} and $d_{\alpha k}$ are determined from the variational consideration $\langle \Psi | \mathcal{H} - E | \Psi \rangle$, where $\mathcal{H}$ is the Hamiltonian and E is the energy, yielding scattering matrices $\mathbf{S}$ and dipole matrices $\mathbf{d}$ that are used to compute photoionization cross sections.

This standard R-matrix approach is modified by the inclusion of an optical potential [6] within MQDT methods [7–10]. The optical potential allows for implicit inclusion of those channels that are left out of the explicit expansion in Eq. (6), whereas MQDT techniques reveal the nearly analytic energy dependence of resonant scattering matrices that are then modified by an additional imaginary energy term. Combination of optical potential and MQDT methods was previously developed in order to include the effect of radiative decay channels in the close-coupling method [11], and was subsequently used to account for radiation damping in electron-impact excitation [12,13] and dielectronic recombination [13–16].

Our treatment of spectator decay is analogous to the treatment of radiative decay of a core state in Ref. [11]. For radiative transitions involving core electronic states, $\Phi_i nl \to \Phi_f nl + h\nu$, the valence electron nl acts as a spectator and the energy of the core ionic state acquires an imaginary term

$$E_i \to E_i - i\Gamma_i/2. \quad (7)$$

Here the partial radiative core decay width Γ_i is given in lowest-order perturbation theory as

$$\Gamma_i = 2\pi \sum_f |\langle \Phi_i | D | \Phi_f \rangle|^2, \quad (8)$$

where D is the dipole operator. Complex core energies for energetically closed channels give rise to complex effective quantum numbers ν, which are determined as $E = E_c - i\Gamma/2 - Z^2/2\nu^2$. A MQDT reduction of all possible channels to the physically allowed open ones [3] then gives a scattering matrix

$$\mathbf{S}_{oo}^{\mathrm{phys}} = \mathbf{S}_{oo} - \mathbf{S}_{oc}(\mathbf{S}_{cc} - e^{-i2\pi\nu})^{-1}\mathbf{S}_{co} \quad (9)$$

that is no longer unitary due to the complexity of ν, and there is an accompanying loss of scattered flux due to decay of the resonances to the implicitly included radiative channels. Likewise, the physical dipole matrix

$$\mathbf{d}^{\dagger,\mathrm{phys}} = \mathbf{d}_o^\dagger - \mathbf{d}_c^\dagger(\mathbf{S}_{cc}^* - e^{i2\pi\nu^*})^{-1}\mathbf{S}_{co}^* \quad (10)$$

gives rise to damped photoionization cross sections.

There are many appealing aspects of using a complex potential, especially for the present case, where the redistribution of flux to spectator Auger decay must be taken into account. First, the prescription in Eq. (7) was suggested by Hickman [17] as a means for implicitly including radiative channels (see also Ref. [18], Sec. 6.11, and Ref. [19], Sects. I.7 and VIII.2.1). Second, a detailed MQDT derivation by Bell and Seaton [20] (see also Ref. [21]) gives a formalism that is an excellent approximation to Eq. (7). Third, the concept of core-excited resonance states having, within the limited close-coupling expansion space, finite lifetimes at the Rydberg limit makes sense physically. Nevertheless, in order to relate this approach to the case of Auger decay of the core, as opposed to radiative decay, we present an alternative derivation of the complex energy result in Appendix A.

Implicit inclusion of spectator Auger decay states, given in Eq. (5), is accomplished by adjusting the core energies in closed channels according to the optical potential result of Eq. (7) using the autoionization width

TABLE I. Ar and Ar^+ energies.

		Theoretical		Experimental	
		Absolute (a.u.)	Relative (eV)	Relative (eV)	Photon Energy (eV)
Ar	$2s^2 2p^6 3s^2 3p^6\ ^1S_0$	-530.849	-18.64	-15.75	0.00
Ar^+	$2s^2 2p^6 3s^2 3p^5\ ^2P^o_{3/2}$	-528.109	0.00	0.00	15.75
	$2s^2 2p^6 3s^2 3p^5\ ^2P^o_{1/2}$	-528.102	0.17	0.18[a]	15.93
	$2s^2 2p^6 3s 3p^6\ ^2S_{1/2}$	-527.626	13.14	13.48[a]	29.23
	$2s^2 2p^5 3s^2 3p^6\ ^2P^o_{3/2}$	-519.521	233.68	232.87	248.62
	$2s^2 2p^5 3s 3p^6\ ^2P^o_{1/2}$	-519.442	235.83	235.02[b]	250.77
	$2s 2p^6 3s 3p^6\ ^2S_{1/2}$	-518.440	263.11		

[a]Reference [24].
[b]Reference [33].

$$\Gamma = 2\pi \sum_{i+j=6} \sum_{l,S_c,L_c} |\langle 2p^5 3s^2 3p^6(^2P)|V| \times 2p^6 3s^i 3p^j(^{2S_c+1}L_c)\epsilon l(^2P)\rangle|^2. \quad (11)$$

Inclusion of the imaginary term causes a broadening of the resonances in the main line cross sections, and in the total photoabsorption spectrum (the energy-averaged resonance contribution to this latter cross section is conserved). An important consequence of using a complex energy is that the photoabsorption cross section is computed in a different manner than simply summing the main line cross sections, because decay, via the optical potential, of resonances to the satellite lines is an important contribution. Following the formulation by Robicheaux [22] of the photoabsorption cross section at complex energies, this can be written as

$$\sigma_{\text{photoabsorption}} = \frac{4\pi^2\omega^q}{3c(2J_0+1)} \text{Re}[\mathbf{d}^\dagger(\mathbf{S}^{-1} - e^{2i\beta})^{-1} \times (\mathbf{S}^{-1} + e^{2i\beta})\mathbf{d}], \quad (12)$$

where $q=1(-1)$ when using the length (velocity) form of the dipole operator, $J_0=0$ for the present closed-shell initial state of Ar, $\mathbf{S}$ is the unphysical scattering matrix, $\mathbf{d}^\dagger$ is the unphysical (with $\mathbf{S}^\dagger$ normalization) dipole matrix, and $\beta = \pi\nu$ for closed channels and $\beta = i\infty$ for open channels. (For the present calculations, we force all channels coupled to the $2p^{-1}$ target states of Ar^+ to be closed even above these thresholds in order to obtain smooth partial cross sections through threshold; otherwise, a discontinuity would arise due to the switching off of the imaginary term in the outer electron's energy above threshold). Note that the approximate Eq. (21) from Ref. [22] is used instead of the exact Eq. (20) since the relative size of the error is roughly $e^{-2\pi/\sqrt{\Gamma}} \sim 10^{-22}$ in the present case. By computing the difference between the above total photoabsorption cross section and the sum of cross sections to the main lines, the satellite cross sections to the spectator Auger decay channels can be determined. This is given in Appendix B.

III. COMPUTATIONAL DETAILS

The most essential details of the *R*-matrix calculation are the following. A physical orbital basis $\{1s,2s,2p,3s,3p\}$ was first generated by performing a Hartree-Fock [23] calculation for the $3p^5(^2P)$ ground state of Ar^+. This orbital basis was augmented by a $\overline{3d}$ pseudo-orbital obtained from a multiconfiguration Hartree-Fock (MCHF) calculation [23] for the $(63\%3s3p^6 + 37\%3s^2 3p^4 \overline{3d})(^2S)$ first excited state, and additional $\overline{4s}$ and $\overline{4p}$ pseudo-orbitals which were used to correct for term dependence of the $2p^5 3s^2 3p^6$ inner-shell excited state. The latter two orbitals were generated by performing a MCHF calculation in which the $3s \rightarrow \overline{4s}$ ($\sim 1\%$) and $3p \rightarrow \overline{4p}$ ($\sim 5\%$) promotions from the $2p^5 3s^2 3p^6$ state were included. The resulting configuration-interaction (CI) expansion for the *LS* target states used 54 configurations consistent with single promotion out of the $3p^5$, $3s3p^6$, and $2p^5 3s^2 3p^6$ states, giving 54 *LS*-coupled channels for the ^1S initial symmetry, 87 for the *LS*-allowed $^1P^o$ final symmetry, and 87 and 33 of these for the *LS*-forbidden $^3P^o$ and $^3D^o$ final symmetries, respectively. Double promotions out of the $3p^5$, $3s3p^6$, and $2p^5 3s^2 3p^6$ states are not considered here since they would lead to a target basis too large for a full *JK*-coupled *R*-matrix calculation (see below and the discussion in Ref. [28]); in addition, these double promotion configurations do not improve significantly the agreement between theoretical and experimental energies (see Table I).

It was necessary to account for spin-orbit effects since, as seen in Table I, there is a 2.15-eV fine-structure splitting between the $2p_{3/2}^{-1}$ and $2p_{1/2}^{-1}$ ionic states. Just as important, the overall resonance behavior differs appreciably from *LS*-coupling predictions, as will be demonstrated in Sec. IV. Spin-orbit effects can often be incorporated through frame transformation methods [3,25–27], as was done recently in a study of photoionization in neon [28], but in the present study this method encountered difficulties near the $2p^{-1}$ thresholds due to the strong energy dependence of the eigenquantum defects (eigenvalues of the reactance matrix **K**). The double-well potential of the $2p^{-1}$ Ar^+ ion gives rise to shape resonances [29] (see also Ref. [18], Chap. 5) that, together with the separation of the core energies by the 2.15-eV fine-structure splitting, leads to inaccurate results. Instead, a full *JK*-coupled calculation was performed, which, due to memory limitations [28], restricted the size of the Ar^+ target state CI expansion.

Coupled to each target configuration are 20 continuum orbitals per channel, resulting in a JK-coupled $J=1^o$ basis consisting of 2400 elements. A Breit-Pauli R-matrix [30,31] calculation was performed, smooth scattering and dipole matrices were obtained using the asymptotic methods detailed earlier [12,14,16], and the MQDT and optical potential methods of Sec. II were applied, generating partial and total photoionization cross sections. The photon energy was shifted by +3.72 eV in order that the theoretical and experimental thresholds coincided; due to the lack of convergence in the *absolute* Ar^+ energies, the Ar ground-state energy is about 2.9 eV too low, and the $2p^{-1}$ inner-shell excited state energies are about 0.8 eV too high, relative to the $3p^{-1}$ ground state of Ar^+ (see Table I). The core autoionization width of Eq. (11) was computed using the program AUTOSTRUCTURE [32] as

$$\Gamma = 2\pi \sum_{i+j=6} \sum_{l,S_c,L_c} |\langle 2p^5 3s^2 3p^6\,(^2P)|V|2p^6 3s^i 3p^j(^{2S_c+1}L_c)\epsilon l(^2P)\rangle|^2 = 4.23\times 10^{-3}\ \text{a.u.}, \tag{13}$$

which is in agreement with the measured values for the entire $2p^{-1}nl$ Rydberg series, where the width varied between about 4×10^{-3} a.u.$<\Gamma<5\times10^{-3}$ a.u. [33]. Intermediate coupling results for the $2p^5 3s^2 3p^6(^2P_{3/2})$ and $2p^5 3s^2 3p^6(^2P_{1/2})$ partial widths differed from this value by less than 1%.

IV. RESULTS AND DISCUSSION

In order to illustrate the effect of including the optical potential term given in Eq. (7), a comparison is made between results obtained with and without this addition in Fig. 1. The optical potential term causes a broadening of the resonances, giving rise to widths that are independent of principal quantum number. It was shown by Robicheaux *et al.* [11] that the usual Fano profile is modified by the presence of additional damping effects, which in our case are the decay routes to spectator channels, with widths Γ_s. In the absence of spectator decay, and considering the case of an isolated resonance with total participator decay width Γ_p, the *total* photoionization cross section is given by the familiar Fano profile [34,35]

$$\sigma = \sigma_a \frac{(q+\epsilon)^2}{1+\epsilon^2} + \sigma_b, \tag{14}$$

where σ_a and σ_b are the direct cross section contributions to continuum spaces that do and do not interact with the resonance, respectively, $\epsilon = 2(E-E_r)/\Gamma_p$ is the energy detuning from resonance, with position E_r; and the Fano q parameter is a function of the dipole and autoionization matrix elements. This analytic function is seen to have a minimum of $\sigma=\sigma_b$ at $E=E_r-q\Gamma_p/2$ and a maximum of $\sigma=\sigma_a(q^2+1)+\sigma_b$ at $E=E_r+\Gamma_p/2q$. In a single-channel case, where $\sigma_b=0$, Robicheaux *et al.* [11] showed in their Eq. (53) that the profile, including the additional spectator decay via an optical potential, is instead

$$\sigma = \sigma_a \frac{\left(q\dfrac{\Gamma_p}{\Gamma_p+\Gamma_s}+\epsilon\right)^2 + \left(\dfrac{\Gamma_s}{\Gamma_p+\Gamma_s}\right)^2}{1+\epsilon^2}, \tag{15}$$

where now $\epsilon = 2(E-E_r)/(\Gamma_p+\Gamma_s)$. The extra damping term Γ_s increases the minimum cross section and decreases the maximum. In the limit $\Gamma_s \gg \Gamma_p$, which is the case as $n\to\infty$ due to the differences in scaling discussed earlier, the cross section is simply $\sigma_a+\sigma_b$, and is devoid of any resonance structure. Such high-n behavior is clearly seen in both *partial* cross sections in Fig. 1.

Partial cross sections in the vicinity of an isolated resonance are more complicated since the individual contributions to the continuum that interacts with the resonance must be unraveled. It was shown by Starace [36] that the partial cross sections show similar Fano profile behavior, for his Eq.

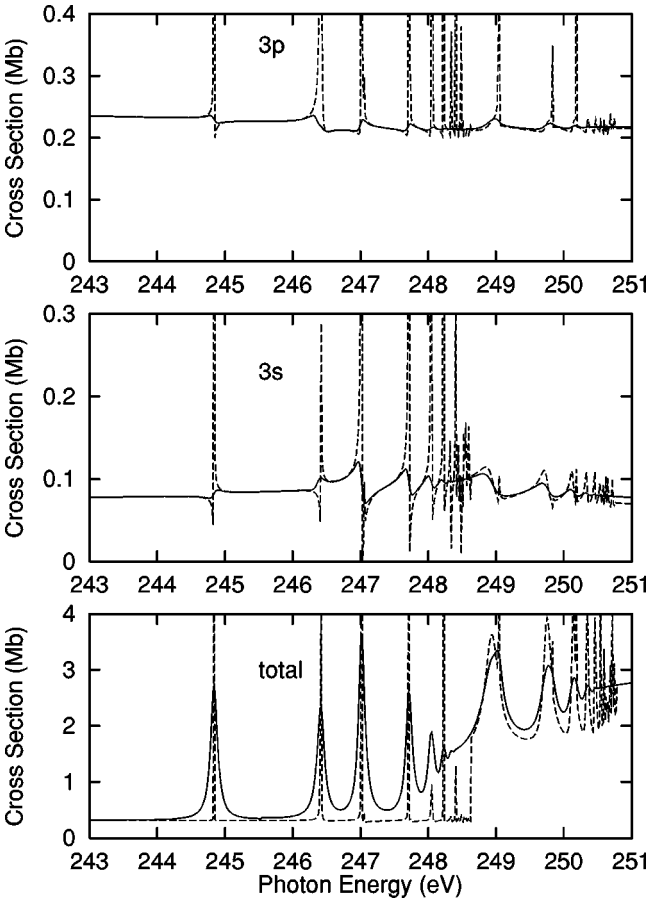

FIG. 1. Comparison between standard (dashed line) and optical potential (solid line) R-matrix results for the argon $3p^{-1}$ and $3s^{-1}$ main lines, and total photoabsorption. All results use the length form of the dipole operator.

TABLE II. $2p^{-1}(^2P_{3/2})4s(J=1^o)$ resonance parameters

$\sigma_{ai}+\sigma_{bi}$	$0.2615-0.004\times(E-244)$ (Mb)
$\frac{\sigma_{ai}}{\sigma_{ai}+\sigma_{bi}}$	0.093
q_i	-350.
E_r	244.8405 (eV)
Γ_p	6.95×10^{-5} (eV)
Γ_s	0.117 (eV)[a]

[a]Computed using AUTOSTRUCTURE [32].

(26) can be rewritten in the form

$$\sigma_i=\sigma_{ai}\frac{(q_i+\epsilon)^2}{1+\epsilon^2}+\sigma_{bi}, \tag{16}$$

where q_i, σ_{ai}, and σ_{bi} are rather complicated functions of the continuum channel (of index i). While an analytic modification of these expressions due to a complex energy is beyond the scope of this paper, it is tempting to try the single-channel prescription of Robicheaux *et al.* [11], that is, to compare the modified expression

$$\sigma_i=\sigma_{ai}\frac{\left(q_i\frac{\Gamma_p}{\Gamma_p+\Gamma_s}+\epsilon\right)^2+\left(\frac{\Gamma_s}{\Gamma_p+\Gamma_s}\right)^2}{1+\epsilon^2}+\sigma_{bi} \tag{17}$$

with the computed R-matrix results for an isolated resonance. The relevant $2p^{-1}(^2P_{3/2})4s$ resonance parameters that reproduce the computed, *undamped* $3p^{-1}$ cross section are given in Table II, and the results in Fig. 2 show that the analytic and computed *undamped* cross sections are in excellent agreement. By using these same parameters and the previously computed core autoionization width $\Gamma_s=0.117$ eV, the above modified expression in Eq. (17) gives excellent agreement with the computed *damped* R-matrix cross section. Note that the undamped cross-section maximum of $\sigma_{ai}(q_i^2+1)+\sigma_{bi}\simeq3\times10^4$ Mb overestimates the ''true'' cross-section maximum by more than five orders of magnitude.

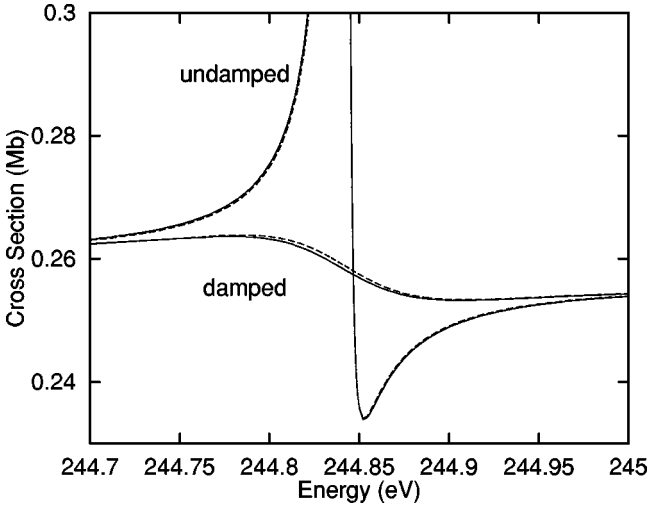

FIG. 2. Parametrization of the $2p^{-1}(^2P_{3/2})4s(J=1^o)$ resonance in the $3p^{-1}$ main line cross section: solid lines, R-matrix results with and without optical potential; dashed lines, analytic forms of Eqs. (16) and (17) using the fitted parameters in Table II (Γ_s is computed using AUTOSTRUCTURE). All results use the length form of the dipole operator.

Another interesting feature of the present results is that, even though the participator channels show massive broadening, clear asymmetries remain that differ between the $2p^{-1}ns$ and $2p^{-1}nd$ resonances. These asymmetries are also seen in the experimental results [37], that are compared to the optical potential results in Fig. 3 for the $3s^{-1}$ main line and the total photoabsorption cross section. The length and velocity theoretical results show almost identical resonance structure, the only noticeable difference being a roughly 15% difference in the $3p$ background cross section. Qualitatively, overall, the theoretical and experimental results agree quite well, showing similar Fano asymmetric resonance profiles and relative oscillator strengths. One exception to this appears in the region $h\nu\approx246.5$ eV. Here the theoretical $2p_{1/2}^{-1}4s$ resonance is quite distinct from the neighboring $2p_{3/2}^{-1}3d$ resonance at $h\nu\approx247$ eV, whereas the experimental results show these two closer together in energy. This difference in relative energy positions is perhaps seen most clearly in the total cross section, and it is probably the reason for the quantitative discrepancy between the $3s^{-1}$ results. For instance, comparison between the theoretical and experimental $3s^{-1}$ cross sections shows that the two resonances overlap more closely in the experiment and therefore give a single feature, unlike the two distinct ones seen in the theoretical results. The largest discrepancy in energy position is for the $2p_{3/2}^{-1}4s$ resonance at $h\nu\approx244.4$ eV experimentally, for which the theoretical result lies instead at $h\nu\approx244.8$ eV, about 0.4 eV too high. We cannot think of what additional effects might be included in the calculation in order to bring this result more in line with experiment, but it should be pointed out that the lowest-lying $4s$ resonances have a valence electron that strongly overlaps with the other target electrons, and are therefore the most difficult to correlate with a limited CI expansion.

Another major quantitative difference exists between the background cross sections. For instance, the computed $3s^{-1}$ cross section is about the same at 243 and 251 eV, whereas the experimental cross section result at 251 eV is roughly twice that at 243 eV. While it is unclear whether or not the discrepancy in this case could be due to experimental uncertainty in the background signal, it should be pointed out that the theoretical background cross section undergoes a rapid variation with energy in the region of the $2p^{-1}$ thresholds. This is due to a shape resonance caused by the double-well potential [29], and it is possible that the energy position of this resonance is not converged in the present calculations.

For the sake of future experimental studies of the participator channels, the theoretical $3p^5(^2P_{J_c})$ photoionization cross section has been resolved into the $J_c=\frac{3}{2}$ and $\frac{1}{2}$ fine-structure levels in Fig. 3. The striking result here is that, contrary to the nonrelativistic prediction that the two should be in proportion to their statistical weights $2J_c+1$ [38], giving a ratio

$$r=\frac{\sigma_{3/2}}{\sigma_{1/2}}=2 \quad \text{(nonrelativistic)}, \tag{18}$$

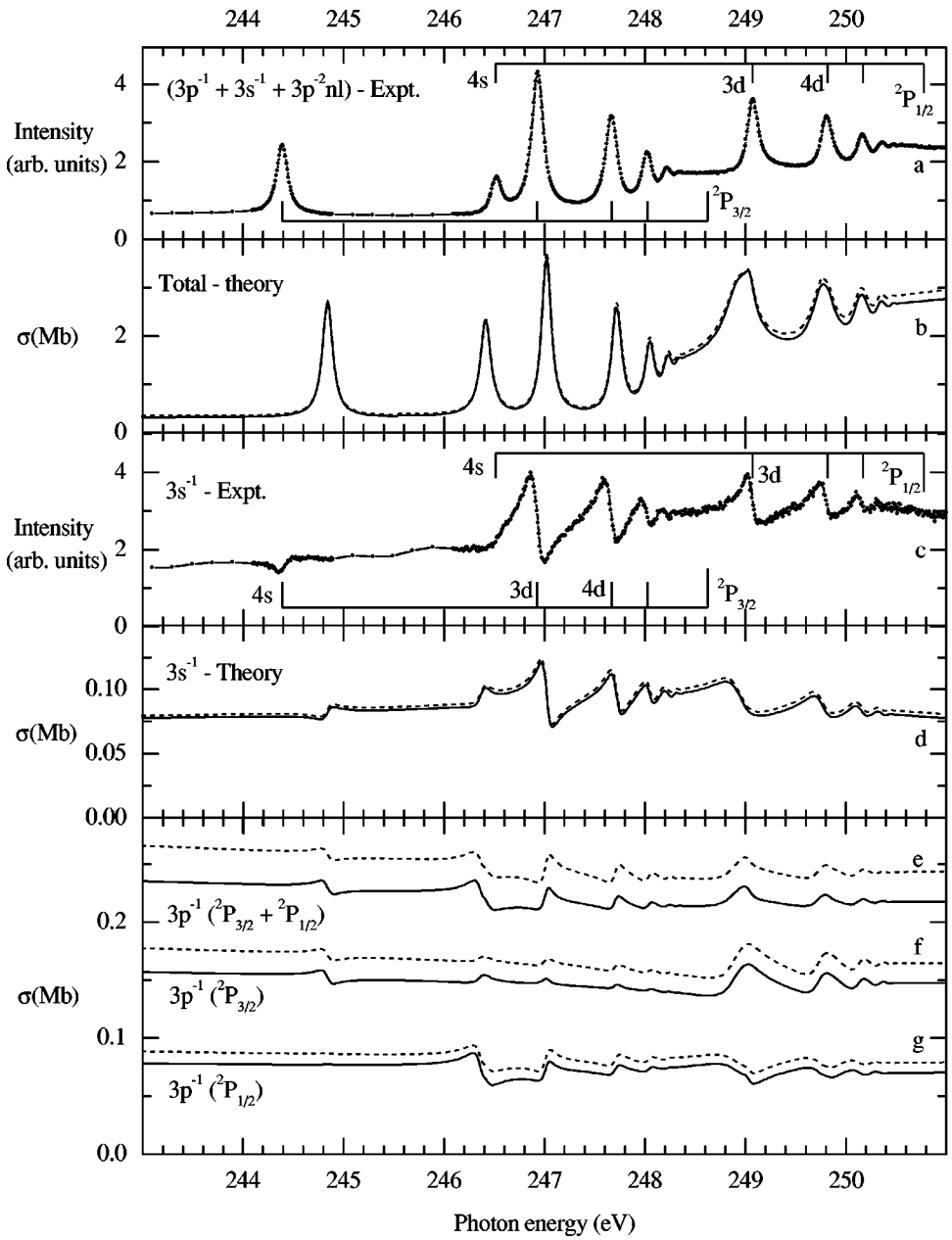

FIG. 3. Comparison between experimental and optical potential *R*-matrix results for partial and total photoionization cross sections. The experimental results in (a) do not include $3s^{-1}3p^{-1}nl$, $3s^{-2}nl$, or $2p^{-1}(^2P_{3/2})$ ionic contributions. The theoretical solid (dashed) curve corresponds to the length (velocity) form of the dipole operator.

there are pronounced differences between the two, with ratios varying from $r \simeq 1.7$ to $r \simeq 2.7$. Even on a qualitative level, there are major differences. First, the $2p^{-1}(^2P_{3/2})4s$ resonance at 244.8 eV only appears in the $3p^5(^2P_{1/2})$ cross section. Second, the asymmetries differ between the two such that there is partial cancellation of resonance features in the summed cross section [see Figs. 3(f) and 3(g), especially in the 249–251 eV region]. Resolution into fine-structure levels therefore gives a more complete picture of the resonance structure.

Recently, Liu and Starace [39] extended the earlier analysis of Starace [36] to prove that in the limit $\rho^2 = \sigma_a/(\sigma_a + \sigma_b) \rightarrow 0$, where σ_a and σ_b are the interacting and noninteracting direct cross sections in Eq. (14), any two groupings of partial cross sections will exhibit mirroring in the resonance behavior, and, as a consequence, the total cross section will be symmetric or Lorentzian. By grouping the present total (participator) cross section into (1) the $3p^{-1}(^2P_{3/2})$ partial cross section and (2) the sum of the $3p^{-1}(^2P_{1/2})$ and $3s^{-1}(^2S_{1/2})$ partial cross sections, mirroring is clearly seen for most of the resonance features in Fig. 4. Since the total undamped *participator* cross section is seen to have a small ρ^2 parameter in Fig. 1, mirroring behavior is expected.

Theoretical angular distribution parameters β are shown in Fig. 5, where major qualitative differences also exist between the $3p^5(^2P_{3/2})$ and $3p^5(^2P_{1/2})$ results, again indicating spin-orbit effects. The $3s3p^6$ β value also varies from the nonrelativistic prediction [40]

$$\beta_{3s} = 2 \quad \text{(nonrelativistic)}, \tag{19}$$

showing a somewhat lower value for the $2p^{-1}(^2P_{1/2})nl$ resonances.

V. CONCLUSION

It has been demonstrated that optical potential methods are able to model the physical broadening of inner-shell ex-

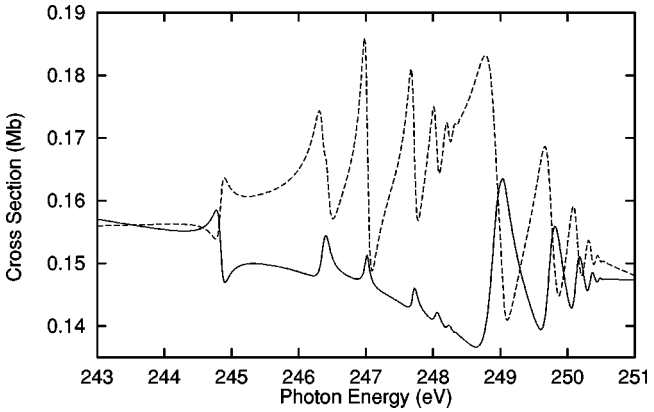

FIG. 4. Comparison of the $\sigma_{2p^{-1}(^2P_{3/2})}$ cross section to the sum of the $\sigma_{2p^{-1}(^2P_{1/2})}+\sigma_{2s^{-1}(^2S_{1/2})}$ cross sections, showing a mirroring of asymmetric features. All results use the length form of the dipole operator.

cited resonances due to spectator Auger decay, and give theoretical resonance widths and relative heights that agree quite well with experimental main line and total photoabsorption results, except where noted due to atomic structure inaccuracies. This method can also be used to extract spectator cross sections, and is detailed in the Appendixes. It appears that the major discrepancy with experiment is due to the unconverged low-lying theoretical resonances positions. This is always a source of error in any *R*-matrix calculation, and does not indicate a deficiency in the present optical potential, MQDT method. But it is noted that certain approximations have been assumed in this theoretical treatment, and require additional studies to ascertain their accuracy. As a further guide for future experiments, fine-structure-resolved cross sections and angular distribution parameters were presented, showing major qualitative departure from nonrelativistic predictions.

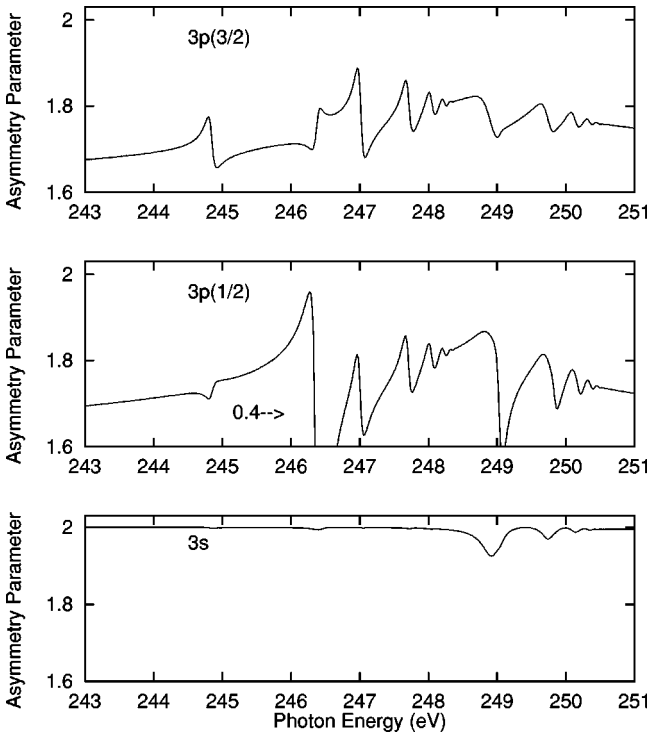

FIG. 5. Asymmetry parameters β to the $3p^5(^2P_{3/2})$, $3p^5(^2P_{1/2})$, and $3s3p^6(^2S_{1/2})$ continua. The solid (dashed) curve corresponds to the length (velocity) form of the dipole operator.

ACKNOWLEDGMENTS

We would like to thank O. Nayandin, A. A. Wills, A. Farhat, M. Alsheri, B. Langer, J. D. Bozek, and N. Berrah for making their experimental results available prior to publication, and C. N. Liu for helpful comments on the asymmetry aspects of the present study. F.R. was supported by a U.S. DOE grant.

APPENDIX A: DERIVATION OF THE SPECTATOR AUGER DECAY OPTICAL POTENTIAL

In order to see the approximations of using an optical potential to include Auger decay, the complex energy close coupling equations are derived in the following manner. The wave function is modified by the addition of satellite continua,

$$\Psi(R,r)=\sum_i \Phi_i(R)f_i(r) + \sum_{j,n}\int d\epsilon\, A_{jn}(\epsilon)\phi_j(R_{-1})g_j(r',\epsilon)h_{nj}(r), \tag{A1}$$

where $\Phi_i(R)$ and $\phi_j(R_{-1})$ are wave functions for the Ar^+ and Ar^{2+} ionic states, respectively; $g_j(r',\epsilon)$ are continuum distorted waves with asymptotic energy $\epsilon>0$ relative to the Ar^{2+} energy E_j^{2+}; $h_{nj}(r)$ are bound distorted waves with relative energy $e_n<0$; and antisymmetrization and angular momentum coupling are implicitly assumed throughout. The distorted waves satisfy the following e^-+Ar^{2+} scattering equations:

$$\int dR_{-1}\phi_k^*(R_{-1})\mathcal{H}(R)\phi_j(R_{-1})g_j(r',\epsilon)=(E_j^{2+}+\epsilon)\delta_{kj}, \tag{A2}$$

$$\int dR_{-1}\phi_k^*(R_{-1})\mathcal{H}(R)\phi_j(R_{-1})h_{nj}(r')=(E_j^{2+}+e_n)\delta_{kj}. \tag{A3}$$

The bound orbitals are orthonormal, $\int dr' h_{nj}^*(r')h_{n'j}(r')=\delta_{nn'}$, and the continuum orbitals are energy normalized, $\int dr' g_j^*(\epsilon',r')g_j(\epsilon,r')=\delta(\epsilon'-\epsilon)$. In what follows, it is assumed that the two outermost electrons in the spectator channels act independently in the second term, so that

$$\int dR_{-1}dr'dr\ \phi_k(R_{-1})g_k(r',\epsilon')h_{mk}(r) \times\mathcal{H}(R,r)\phi_j(R_{-1})g_j(r',\epsilon)h_{nj}(r) =\delta_{mn}\delta_{kj}\delta(\epsilon-\epsilon')(\epsilon+e_n+E_j^{2+}). \tag{A4}$$

The Rydberg electron and the continuum electron are independent to a good approximation because the continuum electron has a high energy, whereas the Rydberg electron can only respond slowly.

The variational condition $\langle \delta\Psi|\mathcal{H}(R,r)-E|\Psi\rangle=0$, where $\mathcal{H}(R,r)=\mathcal{H}(R)+\Sigma_{i=1}^{N-1}(1/r_{i,N})+\mathcal{H}(r)$, yields the following equations satisfied by the undetermined functions $f_i(r)$ and $A_{jn}(\epsilon)$:

$$\int dR\,\Phi_k^*(R)\{\mathcal{H}(R,r)-E\}\Psi(R,r)=\sum_i\{[\mathcal{H}(r)+E_i^+-E]\delta_{ki}+U_{ki}(r)\}f_i(r)+\sum_{j,n}\int d\epsilon\,A_{jn}(\epsilon)\int dR\,\Phi_k^*(R)[\mathcal{H}(R)-E]\phi_j(R_{-1})g_j(r',\epsilon)h_{nj}(r)=0, \tag{A5}$$

$$\int dR dr\,\phi_k^*(R_{-1})g_k^*(r',\epsilon')h_{mk}^*(r)\{\mathcal{H}(R)-E\}\Psi(R,r)=\sum_i\int dR\phi_k^*(R_{-1})g_k^*(r',\epsilon')(\mathcal{H}(R)-E+e_m)\Phi_i(R)\times\left[\int dr\,h_{mk}^*(r)f_i(r)\right]+A_{km}(\epsilon')(\epsilon'+e_m+E_k^{++}-E)=0 \tag{A6}$$

Solving Eq. (A6) for $A_{km}(\epsilon')$ gives

$$A_{km}(\epsilon')=\sum_i\frac{V_{ki}(\epsilon')\langle h_{mk}|f_i\rangle}{\epsilon'+e_m+E_k^{++}-E}, \tag{A7}$$

which, when inserted into Eq. (A5), gives the resulting close-coupling equation

$$\sum_i\left\{[(\mathcal{H}(r)+E_i^+-E)\delta_{ki}+U_{ki}(r)]f_i(r)+\sum_{j,n}\int d\epsilon\left(\frac{V_{ji}(\epsilon)\langle h_{nj}|f_i\rangle}{\epsilon+e_n+E_j^{++}-E}\right)V_{jk}^*(\epsilon)h_{nj}(r)\right\}=0. \tag{A8}$$

Using the pole approximation $\int d\epsilon F(\epsilon)/(\epsilon-x)\simeq -i\pi F(x)$, and assuming $f_i(r)$ can be spanned by the bound functions, $\Sigma_n\langle h_{nj}|f_i\rangle h_{nj}(r)=f_i(r)$, which is a good approximation for the closed-channel orbitals, the close-coupling equations in Eq. (A8) acquire an additional term $-i\pi\Sigma_j V_{ji}(E_i^+-E_j^{2+})V_{jk}^*(E_k^+-E_j^{2+})$. While this matrix includes off-diagonal terms, we omit terms for $i\neq k$ since they account for the unlikely event that the resonance associated with channel i first decays into one of the continua, say channel j, and is then recaptured into resonance state k. Neglecting this small effect, the (closed) channel solutions in Eq. (A5) propagate with complex energy $E-[E_i^+-i\Gamma_i/2]$, where $\Gamma_i=2\pi\Sigma_j|V_{ji}(E_i^+-E_j^{2+})|^2$ is a sum over partial widths. Since this term is only included in the closed channels, the main energy dependence of the $c(r)\sin(\pi\nu)-s(r)\cos(\pi\nu)$ physical solutions is easily modified, leading to the complex energy MQDT expressions in Eqs. (9) and (10).

APPENDIX B: SPECTATOR PHOTOIONIZATION CROSS SECTIONS

Following the MQDT projection onto physical boundary conditions, the total participator photoionization cross section, summed over all open channels, and in units of $4\pi^2\omega^q/3c(2J_0+1)$, takes the form

$$\sigma^{\text{part}}=\mathbf{d}_{\text{phys}}^\dagger\mathbf{d}_{\text{phys}} \tag{B1}$$

$$=(\mathbf{d}_o^\dagger\mathbf{d}_c^\dagger)\begin{pmatrix}\mathbf{1}_{oo}\\ -(\mathbf{S}_{cc}^*-e^{2i\beta^*})^{-1}\mathbf{S}_{co}^*\end{pmatrix}(\mathbf{1}_{oo}\quad -\mathbf{S}_{oc}(\mathbf{S}_{cc}-e^{-2i\beta})^{-1})\begin{pmatrix}\mathbf{d}_o\\ \mathbf{d}_c\end{pmatrix} \tag{B2}$$

$$=\mathbf{d}^\dagger\begin{pmatrix}\mathbf{1}_{oo} & -\mathbf{S}_{oc}(\mathbf{S}_{cc}-e^{-2i\beta})^{-1}\\ -(\mathbf{S}_{cc}^*-e^{2i\beta^*})^{-1}\mathbf{S}_{co}^* & (\mathbf{S}_{cc}^*-e^{2i\beta^*})^{-1}(\mathbf{1}_{cc}-\mathbf{S}_{cc}^*\mathbf{S}_{cc})(\mathbf{S}_{cc}-e^{-2i\beta})^{-1}\end{pmatrix}\mathbf{d}, \tag{B3}$$

where the symmetry relation $\mathbf{S}=\mathbf{S}^{\dagger *}$ and the unitary relation $\mathbf{S}^\dagger\mathbf{S}=\mathbf{1}$ are used to obtain the result $\mathbf{S}_{co}^*\mathbf{S}_{oc}=\mathbf{1}_{cc}-\mathbf{S}_{cc}^*\mathbf{S}_{cc}$.

The total photoabsorption cross section is given instead by Eq. (12), and can be written as

$$\sigma^{\rm tot} = {\rm Re}\,\mathbf{d}^\dagger(1+\mathbf{S}e^{2i\beta})(1-\mathbf{S}e^{2i\beta})^{-1}\mathbf{d} \tag{B4}$$

$$= {\rm Re}\,\mathbf{d}^\dagger \begin{pmatrix} \mathbf{1}_{oo} & \mathbf{S}_{oc}e^{2i\beta} \\ \mathbf{0}_{co} & \mathbf{1}_{cc}+\mathbf{S}_{cc}e^{2i\beta} \end{pmatrix} \begin{pmatrix} \mathbf{1}_{oo} & \mathbf{S}_{oc}e^{2i\beta}(\mathbf{1}_{cc}-\mathbf{S}_{cc}e^{2i\beta})^{-1} \\ \mathbf{0}_{co} & (\mathbf{1}_{cc}-\mathbf{S}_{cc}e^{2i\beta})^{-1} \end{pmatrix} \mathbf{d} \tag{B5}$$

$$= {\rm Re}\,\mathbf{d}^\dagger \begin{pmatrix} \mathbf{1}_{oo} & 2\mathbf{S}_{oc}e^{2i\beta}(\mathbf{1}_{cc}-\mathbf{S}_{cc}e^{2i\beta})^{-1} \\ \mathbf{0}_{oc} & (\mathbf{1}_{cc}+\mathbf{S}_{cc}e^{2i\beta})(\mathbf{1}_{cc}-\mathbf{S}_{cc}e^{2i\beta})^{-1} \end{pmatrix} \mathbf{d} \tag{B6}$$

$$= \mathbf{d}^\dagger \begin{pmatrix} \mathbf{1}_{oo} & -\mathbf{S}_{oc}(\mathbf{S}_{cc}-e^{-2i\beta})^{-1} \\ -(\mathbf{S}^*_{cc}-e^{2i\beta^*})^{-1}\mathbf{S}^*_{co} & (\mathbf{S}^*_{cc}-e^{2i\beta^*})^{-1}(e^{2i(\beta^*-\beta)}-\mathbf{S}^*_{cc}\mathbf{S}_{cc})(\mathbf{S}_{cc}-e^{-2i\beta})^{-1} \end{pmatrix} \mathbf{d}, \tag{B7}$$

where the last step used the relation ${\rm Re}\,\mathbf{d}^\dagger\mathbf{X}\mathbf{d} = \frac{1}{2}\mathbf{d}^\dagger(\mathbf{X}+\mathbf{X}^\dagger)\mathbf{d}$. Partitioning $\mathbf{d}$ into open and closed components, the additional contribution to the total photoabsorption cross section absent from the participator expression can be computed as

$$\sigma^{\rm spect} = \sigma^{\rm tot} - \sigma^{\rm part} = \mathbf{d}_c^\dagger(\mathbf{S}^*_{cc}-e^{2i\beta^*})^{-1}(e^{2i(\beta^*-\beta)}-1)(\mathbf{S}_{cc}-e^{-2i\beta})^{-1}\mathbf{d}_c \tag{B8}$$

$$= \mathbf{D}^\dagger(e^{4Im\,(\beta)}-1)\mathbf{D}. \tag{B9}$$

This term is just the cross section to the spectator channels, and can be reduced to an incoherent contribution from each of the closed channels. By considering the branching ratios for autoionization of each closed-channel resonance into the accessible Ar^{2+} final continuum states, $\Gamma_{ji}/\Sigma_k\Gamma_{ki}$, and the inclusion of shake in lowest order [41], which involves the overlap between closed-channel orbitals in the initial resonance state and the bound distorted wave orbitals in the final ionic states, $|\langle h_n|f_i\rangle|^2$, the spectator cross sections can be computed as

$$\sigma^{\rm spect}_{jn} = \sum_i \sum_{l_i} \left| (\mathbf{D})_{i,l_i}{}^2 (e^{4\,{\rm Im}(\beta_i)}-1)\frac{\Gamma_{ji}}{\sum_k \Gamma_{ki}} \right| \langle h_n|f_i\rangle|^2, \tag{B10}$$

where the sum over l_i includes all channels coupled to the particular ionic state i. Note that $\Sigma_{jn}\sigma^{\rm spect}_{jn} = \sigma^{\rm spect}$. The expression in Eq. (B10) is a difficult quantity to compute, however, since there are an infinite number of j and n, and a realistic evaluation of the $\langle h_n|f_i\rangle$ is difficult. Therefore, further studies of the applicability of this method are needed, preferably on simpler systems such as the $1s^{-1}2s^2np$ resonances in Be, the $1s^{-1}2s^22p^6np$ resonances in Ne, or or the $2p^{-1}3s^2np$ resonances in Mg, where LS coupling can be assumed in the first two cases, and the spectator decay channels for a given final n are far fewer in the first and third cases, compared to Ar.

[1] A. F. Starace, *Theory of Atomic Photoionization*, edited by W. Mehlhorn, Handbuch der Physik Vol. 31 (Springer, Berlin, 1982), pp. 1–121.
[2] V. Schmidt, Rep. Prog. Phys. **55**, 1483 (1992).
[3] M. Aymar, C. H. Greene, and E. Luc-Koenig, Rev. Mod. Phys. **68**, 1015 (1996).
[4] M. J. Seaton, Proc. R. Soc. London, Ser. A **218**, 400 (1953).
[5] P. G. Burke and K. A. Berrington, *Atomic and Molecular Processes: An R-matrix Approach* (Institute of Physics, Bristol, 1993).
[6] H. Feshbach, Ann. Phys. (N.Y.) **5**, 357 (1958); **19**, 287 (1962).
[7] M. J. Seaton, Proc. Phys. Soc. London **88**, 801 (1966).
[8] M. J. Seaton, Rep. Prog. Phys. **46**, 167 (1983).
[9] C. H. Greene, U. Fano, and G. Strinati, Phys. Rev. A, **19**, 1485 (1979).
[10] C. H. Greene, A. R. P. Rau, and U. Fano, Phys. Rev. A **42**, 5773 (1982).
[11] F. Robicheaux, T. W. Gorczyca, M. S. Pindzola, and N. R. Badnell, Phys. Rev. A **52**, 1319 (1995).
[12] T. W. Gorczyca, F. Robicheaux, M. S. Pindzola, and N. R. Badnell, Phys. Rev. A **52**, 3852 (1995).
[13] T. W. Gorczyca and N. R. Badnell, J. Phys. B **29**, L283 (1996).
[14] T. W. Gorczyca, F. Robicheaux, M. S. Pindzola, and N. R. Badnell, Phys. Rev. A **54**, 2107 (1996).
[15] T. W. Gorczyca and N. R. Badnell, Phys. Rev. Lett. **79**, 2783 (1997).
[16] N. R. Badnell, T. W. Gorczyca, and A. D. Price, J. Phys. B **31**, L239 (1998).
[17] A. P. Hickman, J. Phys. B **17**, L101 (1984).
[18] J. P. Connerade, *Highly Excited Atoms* (Cambridge University Press, Cambridge, 1998).
[19] N. F. Mott and H. S. W. Massey, *The Theory of Atomic Collisions*, 3rd ed. (Clarendon, Oxford, 1965).
[20] R. H. Bell and M. J. Seaton, J. Phys. B **18**, 1589 (1985).
[21] F. Robicheaux, J. Phys. B **31**, L109 (1998).
[22] F. Robicheaux, Phys. Rev. A **48**, 4162 (1993).
[23] C. Froese Fischer, Comput. Phys. Commun. **64**, 369 (1991).
[24] *Atomic Energy Levels*, edited by C. E. Moore, Natl. Bur. Stand. U. S. Circ. No. 467 (U.S. GPO, Washington, DC, 1949), Vol. I.
[25] U. Fano, Phys. Rev. A **2**, 353 (1970).

[26] K. T. Lu, Phys. Rev. A **4**, 579 (1971).
[27] C. M. Lee and K. T. Lu, Phys. Rev. A **8**, 1241 (1973).
[28] T. W. Gorczyca, Z. Felfli, H.-L. Zhou, and S. T. Manson, Phys. Rev. A **58**, 3661 (1998).
[29] A. R. P. Rau and U. Fano, Phys. Rev. A **167**, 7 (1968).
[30] K. T. Taylor and N. S. Scott, J. Phys. B **14**, L237 (1981).
[31] K. A. Berrington, W. B. Eissner, and P. H. Norrington, Comput. Phys. Commun. **92**, 290 (1995).
[32] N. R. Badnell, J. Phys. B **19**, 3827 (1986).
[33] G. C. King, M. Tronc, F. H. Read, and R. C. Bradford, J. Phys. B **10**, 2479 (1977).
[34] U. Fano, Phys. Rev. **124**, 1866 (1961).
[35] U. Fano and J. W. Cooper, Phys. Rev. **137**, A1364 (1965).
[36] A. F. Starace, Phys. Rev. A **16**, 231 (1977).
[37] O. Nayandin, A. A. Wills, A. Farhat, M. Alsheri, B. Langer, J. D. Bozek, and N. Berrah (unpublished).
[38] See, for example, A. R. P. Rau, in *Electron and Photon Interactions with Atoms*, edited by H. Kleinpoppen and M. R. C. McDowell (Plenum, New York, 1976), p. 141.
[39] C. N. Liu and A. F. Starace, Phys. Rev. A **59**, 1731 (1999).
[40] See, for example, S. T. Manson and A. F. Starace, Rev. Mod. Phys. **54**, 389 (1982).
[41] T. Åberg, Ann. Acad. Sci. Fenn., Ser. AI: Math. **6**, 308 (1969).